Fluid Dynamics & Materials Processing

Tech Science Press

DOI: 10.32604/fdmp.2024.056516

ARTICLE

Quantitative Effects of Velocity and Residual Pressure Level on Aerodynamic Noise of Ultra-High-Speed Maglev Trains

Lanxi Zhang[1], Yuming Peng[1] and Yudong Wu[2,*]

[1]School of Mechanical Engineering, Southwest Jiaotong University, Chengdu, 610031, China

[2]School of Intelligent Manufacturing, Chengdu Technological University, Chengdu, 610031, China

[*]Corresponding Author: Yudong Wu. Email: ydwu@swjtu.edu.cn

Received: 24 July 2024 Accepted: 26 September 2024 Published: 24 January 2025

ABSTRACT

The challenge of aerodynamic noise is a key obstacle in the advancement of low-pressure tube ultra-high-speed maglev transportation, demanding urgent resolution. This study utilizes a broadband noise source model to perform a quantitative analysis of the aerodynamic noise produced by ultra-high-speed maglev trains operating in low-pressure environments. Initially, an external flow field calculation model for the ultra-high-speed maglev train is presented. Subsequently, numerical simulations based on the broadband noise source model are used to examine the noise characteristics. The impact of the train speed and pressure level on noise generation is investigated accordingly. Subsequently, a correlation formula is derived. The results reveal that the amplitude of sound source changes in the streamlined region of the head and tail cars of the train is large, and the amplitude of changes for the middle car is smaller. The noise source strength increases with speed, with a quadrupole noise source becoming dominant when the train speed exceeds 600 km/h. At a speed of 1000 km/h, the noise source intensity from the streamlined area at the rear of the train overcomes that at the front. Furthermore, the noise source decreases as the pressure level in the tube decreases. When the pressure level drops to 0.01 atm, the quadrupole noise source intensity of a train running at 600 km/h significantly weakens and falls below that of the dipole noise source.

KEYWORDS

Low-pressure tube; aerodynamic noise; train speed; quantitative analysis

1 Introduction

With the rapid advancement of technology, societal life has accelerated, leading to increasing demands for faster and more convenient transportation. By the end of 2022, China's high-speed rail network achieved a total operational mileage of 42,000 kilometers, solidifying its status as the greatest globally. This development represents the most rapid, secure, and stable period in the history of railway expansion, significantly enhancing travel efficiency. However, as society progresses, energy limitations have emerged as a global concern, rendering the enhancement of transportation efficiency a universal goal. Traditional wheel-rail trains encounter constraints stemming from pantograph-catenary interaction, aerodynamic drag, aerodynamic noise, and wheel-rail adhesion issues [1–3], preventing them from achieving higher speeds. The fundamental principle of a low pressure pipeline system involves creating a sealed pipeline and employing pumping apparatus to lower the air pressure within the pipeline, thereby generating an operational environment with diminished medium density. This reduction in air resistance and aerodynamic noise during train operation subsequently enhances train velocity. Ultra-high-speed low pressure tube maglev transportation provides a low-density, low-pressure enclosed environment, freeing maglev trains from the constraints of dense atmosphere and reducing aerodynamic effects during high-speed operation, thus facilitating ultra-high-speed travel on the ground [4]. As a result, low-low pressure tube ultra-high-speed maglev transportation has become an important development direction for future environmentally friendly, energy-efficient, and ultra-high-speed transportation technology. Although the sparse air within the tube reduces aerodynamic noise to a degree, the noise itself escalates dramatically, following a power law ranging from the sixth to the eighth power of the train's speed [5,6]. When the train speed surpasses 600 km/h or even exceeds 1000 km/h, the ultra-high-speed maglev system within low-pressure tubes will still generate high-amplitude broadband noise. This diminishes the system's economic efficiency and adversely impacts both the acoustic comfort within the train and the exterior acoustic environment. Therefore, addressing the challenge of aerodynamic noise is crucial for the progression of ultra-high-speed maglev transit within low-pressure tubes.

Extensive research has been conducted on the noise characteristics of high-speed trains, providing valuable insights for investigating the noise of ultra-high-speed maglev transportation in low-pressure tubes. Liu et al. [7] utilized the Lighthill Analogy and Large Eddy Simulation (LES) methods to investigate surface aerodynamic noise emitted by high-speed trains at different velocities. Their research revealed that the dipole sound power of the train scales proportionally to the sixth power of its speed. Tan et al. [8] conducted numerical simulations to examine the flow field and acoustic field of high-speed trains under different ground effect conditions. Their research revealed that both the moving ground and rotating wheels significantly affect the aerodynamic noise at the bottom of the train, with the impact of rotating wheels being less pronounced than that of the moving ground. Shi et al. [9] conducted a comparative analysis on the impact of various simplified models and boundary conditions on aerodynamic noise in the front car and bogie regions of high-speed trains. They concluded that when the head car serves as the source surface, the outcomes of the car body shortened model and the three-car grouping model exhibit greater consistency. Tian et al. [10] investigated the acoustic characteristics of high-speed train bodies and pantographs by varying the scale of numerical models in their study. Their research revealed that while altering the model scale affects the aerodynamic noise propagation characteristics, it does not impact the overall sound pressure level. There is a tendency for the radiated noise energy to shift from lower frequencies to mid-to-high frequencies as the model scale decreases.

Research into aerodynamic noise of low-pressure tube maglev trains has been largely underdeveloped, with corresponding research outcomes somewhat limited. Liu et al. [11] investigated the impacts of pipeline pressure, train velocity, and blockage ratio on dipole and quadrupole noise sources in high-speed, low-pressure tube trains. They observed that as train velocity increases, quadrupole noise sources become increasingly pronounced. Reducing pipeline pressure and blockage ratio effectively mitigates the intensity of aerodynamic noise sources at high speeds. Zhang et al. [12] analyzed the distribution patterns and acoustic metrics such as spectral characteristics of far-field aerodynamic noise within low-pressure pipelines generated by high-speed trains. Their study revealed a direct correlation between train surface pulsating pressure and resultant aerodynamic noise levels, indicating that higher surface pulsations lead to increased sound pressure. Jiali et al. [13] employed statistical energy analysis to establish a numerical simulation model for predicting aerodynamic noise inside high-speed maglev trains within low-pressure environments. They found that aerodynamic noise within these trains exhibits higher levels at the front and rear cars compared to the middle cars, with predominant energy distribution occurring with mid-to-low frequency range.

Research on the aerodynamic noise of low-pressure tube maglev trains began relatively late. The challenges in precisely reproducing the intricate acoustic field in a high-speed, low-pressure, rarefied gas environment, coupled with the lack of experimental conditions to measure essential physical parameters, have resulted in limited research outcomes in this area. The noise mechanism are not yet fully comprehended, and studies on noise characteristics predominantly involve qualitative analyses. Quantitative analysis of the aerodynamic noise characteristics in ultra-high-speed maglev trains within low-pressure pipelines may yield particular data references for advancing related research efforts, thereby reducing redundancy and improving efficiency. This research also holds significant implications for further elucidating noise mechanisms and exploring noise control methods. Therefore, this study employs numerical simulation to quantitatively investigate the impact of train operating speed and pipeline low pressure level on the aerodynamic noise of ultra-high-speed low pressure tube magnetic levitation trains. Initially, a relevant calculation model for the external flow field is constructed based on the flow field characteristics of ultra-high-speed maglev trains operating within low-pressure pipelines. Subsequently, the numerical simulation results of the flow field are analyzed, incorporating a wide-frequency band noise source model to examine the noise characteristics of the trains. Furthermore, the study examines the impact of train operating speed and pipeline low pressure on the longitudinal distribution pattern of sound sources along the train body axis. Finally, mathematical equations linking noise to train operating speed and low-pressure levels are developed based on the noise source results under various influencing conditions, consequently offering significant insights for engineering applications.

2 Numerical Method

2.1 Mathematical Model

In low-pressure tubes, where gas pressure is subnormal, gas density diminishes as tube pressure lowers, resulting in a more significant rarefaction impact of the gas. The degree of gas rarefaction is generally measured by the Knudsen number [14], expressed as follows:

$$Kn = \frac{\lambda}{L} \tag{1}$$

In the equation, The mean free route of air molecules, denoted by λ, denotes the average distance traveled by a molecule between collisions. L represents the characteristic length of the flow, which is taken as the height of the train body, 0.32 m. Gas flow is classified into four primary regimes according to the Knudsen number [15]: the continuum regime ($Kn < 0.01$), the slip flow regime ($0.01 < Kn < 0.1$), the transition regime ($0.1 < Kn < 10$), and the free molecular flow regime ($Kn > 10$). In the continuum regime, gas flow can be accurately characterized using a continuum medium model.

Under the simulated operating parameters of this study, the minimum internal pressure of the tube is 0.01 atm, and the internal environmental temperature is 300 K. Under these conditions, the maximum Knudsen number is:

$$Kn_{\max} \approx 2.35 \times 10^{-5} \ll 0.01 \tag{2}$$

Therefore, under all simulated operating conditions in this study, the fluid within the tube may be categorized as a continuum medium.

At high speeds within a low-pressure tube, the adjacent fluid demonstrates intricate turbulent dynamics. In fluid dynamics calculations, the fluid's compressibility must be considered when the Mach number surpasses 0.3 [16]. The operating speed of the low-pressure tube maglev train studied in this paper ranges from 600 to 1000 km/h, corresponding to a Mach number range of 0.49 to 0.82. Therefore, the flow field is characterized by the three-dimensional compressible Navier-Stokes equations, with air treated as an ideal gas. The k-epsilon two-equation turbulence model, introduced by Shih et al. [17], is widely employed in industrial computational fluid dynamics. The realizable k-epsilon model, which delivers enhanced accuracy and superior alignment with the physical properties of turbulence relative to the standard k-epsilon model, yields more dependable precision in simulating intricate flow fields, including rotating flows, boundary layer flows with significant pressure gradients, and secondary flows. Therefore, this work selected the realizable k-epsilon model for flow field computations to tackle the low-pressure, high-speed flow conditions in low-pressure tubes [18].

The principal sources of aerodynamic noise in the flow field are monopole, dipole, and quadrupole sources [19,20]. This study's numerical calculations, utilizing wind tunnel models, assume the train body's surface is rigid. In real situations, train surfaces often do not undergo much displacement [21]. Therefore, this study primarily analyzes the dipole and quadrupole acoustic sources, excluding the influence of monopole sources to noise. The broadband noise source model for near-field noise prediction employs flow field data derived from Reynolds-Averaged Navier-Stokes (RANS) simulations to ascertain the position and magnitude of major noise sources. This method is advantageous due to its shorter computation time and higher efficiency This approach is beneficial owing to its reduced computing time and enhanced efficiency.

The Curle model assesses the local acoustic power of dipole noise sources. Dipole noise sources arise from the interaction of an object surface in a flow field with an air stream. The radiated power of these noise sources is proportional to the sixth power of the flow velocity:

$$w_d \propto \rho_0 D^2 \frac{v^6}{c_0^3} \tag{3}$$

In the equation, w_d represents the radiated power of the dipole noise source, ρ_0 indicates the density of the flow field, and D denotes the characteristic length of the noise source. The total sound power radiated by a solid surface, P_{SA}, can be approximated as [22]:

$$P_{SA} = \int \frac{A_c(y)}{12\rho_0 \pi c_0^3} \left[\frac{\partial p}{\partial t}\right]^2 dS(y) = \int I(y) dS(y) \tag{4}$$

In the equation, A_c represents the associated region, S denotes the solid surface, and $I(y)$ indicates the dipole noise sources on the solid surface in a flow field.

The surface sound power level is expressed as:

$$L_{SAP} = 10 \log \frac{P_{SA}}{P_{ref}} \tag{5}$$

In the formula, L_{SAP} represents the surface sound power level, and P_{ref} denotes the reference sound power, where $P_{ref} = 10^{-12}$ W/m^2.

The Proudman model evaluates the local power of quadrupole noise sources. Quadrupole noise sources are caused by viscous stresses resulting from the interaction between fluids. The radiated power of these noise sources is proportional to the eighth power of the flow velocity:

$$w_q \propto \rho_0 D^2 \frac{v^8}{c_0^5} \tag{6}$$

In the formula, w_q represents the radiated power of the quadrupole noise source.

The sound power P_A produced per unit volume by quadrupole noise sources in isotropic turbulence is expressed as [23]:

$$P_A = \alpha\rho_0\left(\frac{u^3}{l}\right)\frac{u^5}{c_0^5} \tag{7}$$

In the formula, u represents the turbulence velocity, l shows the turbulence length scale, while α denotes the model constant.

The sound power level is expressed as:

$$L_{AP} = 10\log\frac{P_A}{P_{ref}} \tag{8}$$

In the equation, L_{AP} represents the sound power level, and P_{ref} denotes the reference sound power, where $P_{ref} = 10^{-12}$ W/m^3.

2.2 Numerical Model

This study utilizes a 1:10 scale model train, simplifying complex components such as the pantograph, windshields, and bogies due to computing limitations. The model consists of a three-car configuration (head, middle, and tail) and measures 5 m in length, with a maximum width of 0.37 m and a height of 0.32 m (refer to Fig. 1). A cylindrical geometric model, positioned at the middle height of the train body, features a blockage ratio of 0.11 with a radius (R) of 0.65 m. The total length of the tube is set to 40 m, with the front of the train positioned 10 m from the tube entrance. To avert backflow, a space of 30 m is preserved between the train's front and the tunnel outlet [18].The levitation height of the train is 0.037 m, and the train-tube model is depicted in Fig. 2. A monitoring line (Line 1) is positioned along the longitudinal centerline of the train body, at the midline above the train's surface, to evaluate the distribution of sound power levels released by the train, as seen in Fig. 3.

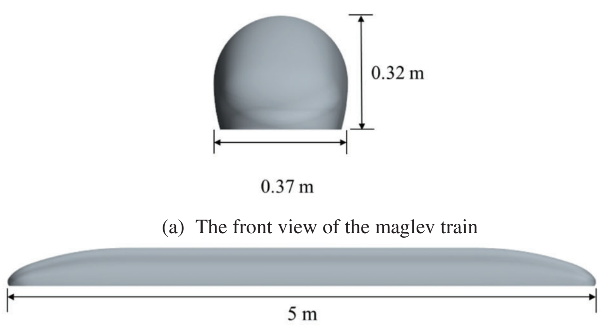

(a) The front view of the maglev train

(b) The side view of the maglev train

Figure 1: Maglev train model

This study analyzes a steady-state flow field. Assuming that the train remains stationary during the numerical simulation, the inlet boundary velocity is modified to simulate the train's continuous motion through the tube. The free-flow boundary (non-reflective Riemannian boundary) is employed at the pipe's intake and outlet to facilitate the natural exit of fluid while preserving continuity and stability in the fluid dynamics of the computational domain. The train is depicted as a stationary no-slip surface, but the pipeline is characterized as a dynamic no-slip wall, with its velocity corresponding to the airflow speed in the wind tunnel model. Additionally, both the train and pipeline walls experience adiabatic thermal boundary conditions.

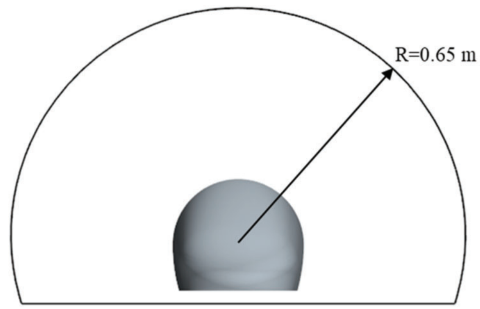

(a) The front view of the computational domain

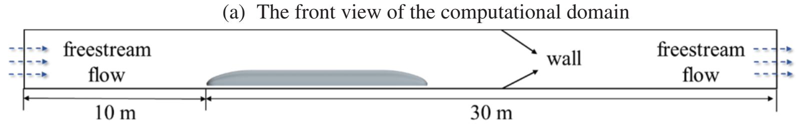

(b) The side view of the computational domain

Figure 2: Simulation model of a maglev train in a low-pressure tube

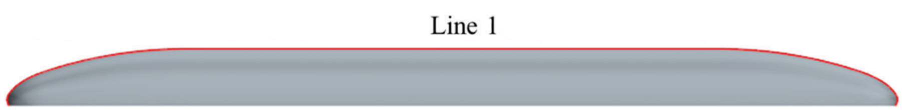

Figure 3: Surface monitoring lines on the train

This study examines train speeds ranging from 600 to 1000 km/h within a low-pressure pipeline. The low-pressure conditions inside the pipeline are simulated by adjusting the internal air pressure, which ranges from 0.1 to 0.01 atm. The initial ambient temperature within the pipeline is set at 300 K.

2.3 Mesh Generation

The numerical simulation employs an unstructured hybrid mesh. Triangular meshes facilitate surface reconstruction for both the train and the pipeline, whereas hexahedral meshes are utilized for discretizing the computational domain of the train. High-resolution meshing is essential near the train body during aerodynamic noise numerical calculations to accurately represent the flow characteristics within the boundary layer. Specifically, the train surface is discretized with a detailed boundary layer mesh consisting of 12 layers, a growth factor of 1.2, and the total boundary layer thickness is set to 4 mm. Additionally, the surface mesh is further improved around the train body, with multiple refinement blocks located near the front and rear cars. The volumetric mesh is additionally improved in certain areas. Fig. 4 depicts the mesh configuration for a maglev train-pipeline model, distinguished by a blockage ratio of 0.11.

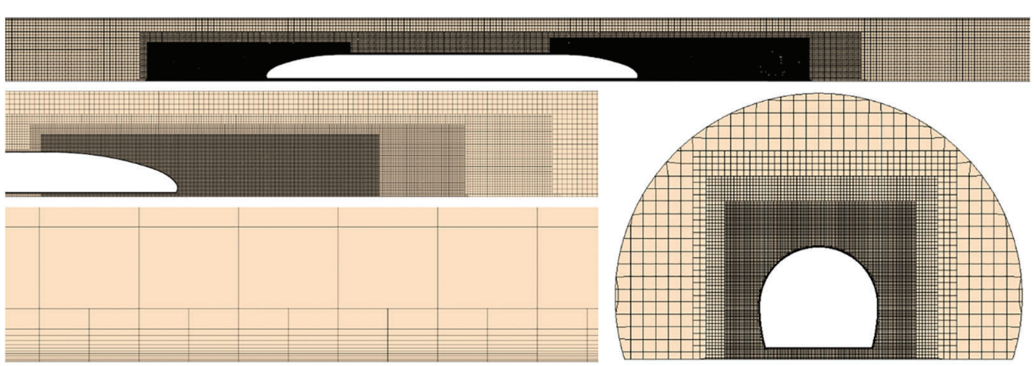

Figure 4: Computational mesh

To achieve mesh independence, three mesh sets with consistent methods but differing densities were created by modifying the mesh resolution of the computational domain. The meshes consisted of 7.03, 16.70, and 26.30 million elements, respectively. Table 1 compares the aerodynamic drag values for the complete vehicle with the dipole noise source value at a specific location on the intermediate car surface for these three mesh sizes. The results demonstrate that the aerodynamic drag values derived from the medium-density mesh show negligible differences when compared to those obtained from the fine mesh. After evaluating computational efficiency and correctness, the medium-density mesh was selected for the further calculations. This meshing approach preserves the y+ values across most of the train's surface within the range of 1 to 30, conforming to the specifications of the realizable k-epsilon two-layer model. Fig. 5 illustrates the distribution of the y+ values.

Table 1: Mesh independence test

Mesh	Mesh number/million	Aerodynamic drag/N	Dipole noise source/dB
Coarse	7.03	61.66	89.80
Medium	16.70	60.86	89.27
Fine	26.30	60.30	89.03

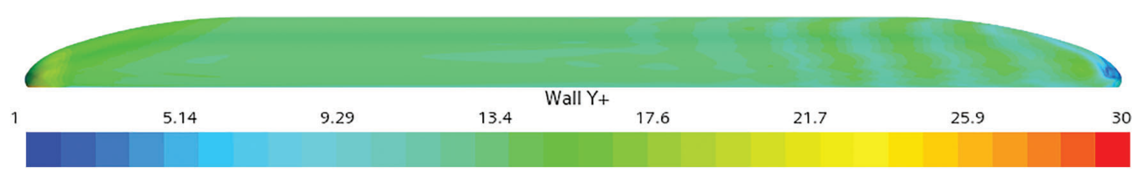

Figure 5: The y+ distribution on the train surface

2.4 Numerical Simulation Verification

This study confirms the numerical approach and mesh accuracy by comparing simulation results with surface pressure data from wind tunnel measurements on a maglev train, given the close link between dipole and quadrupole noise sources and the train's surface pressure [24,25]. Fig. 6 presents the comparison results of the train surface pressure coefficient. The formula used to determine the surface pressure coefficient of the train is as follows:

$$C_p = \frac{P}{0.5\rho_0 v^2} \tag{9}$$

In the above-mentioned formula, P represents the surface pressure on the train, C_p denotes the pressure coefficient, ρ_0 stands for the air density, and v signifies the speed of the train.

The numerical simulation results, as illustrated in the Fig. 6, closely align with the wind tunnel test data, exhibiting variances typically within 5%, thereby satisfying the engineering accuracy standards. Consequently, the numerical simulation method employed in this work is confirmed to be valid.

2.5 Noise Model Verification

To enhance the validation of the noise source model's accuracy, the aerodynamic noise produced by a high-speed train traversing the tunnel beneath Chengdu Tianfu Airport Station was chosen as a reference case. The train was moving at a velocity of 350 km/h through a tunnel with a cross-sectional area of approximately 100 m^2. The measurement points, as illustrated in Fig. 7, were positioned at three locations: Point A (on the windward side of the driver's cabin), Point B (on the left sidewall of the sightseeing portion), and Point C (on the left rear sidewall of the passenger compartment). A numerical simulation model was created under conditions that mirrored the experiment. Table 2 delineates a comparison between the experimental data and the results of the numerical simulation. The table indicates that, owing to surface effects throughout the experiment, the numerical simulation results were generally lower than the experimental measurements, with a maximum divergence of 1.76 dB. This inconsistency indicates that the noise model utilized in this research is rather precise.

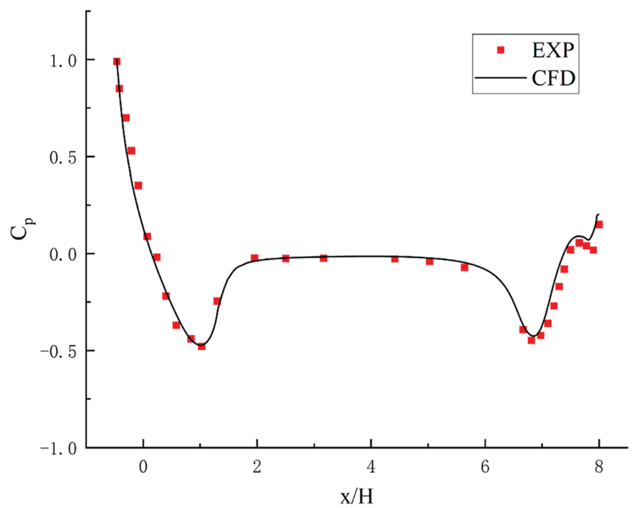

Figure 6: Pressure coefficient comparison

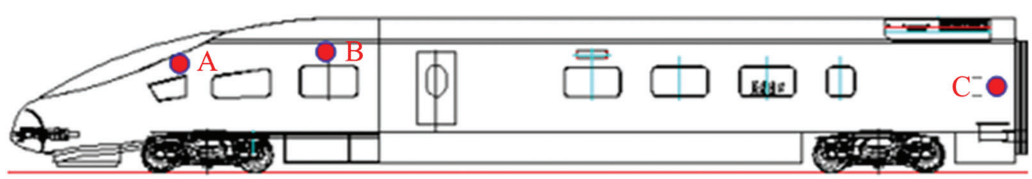

Figure 7: Arrangement of experimental points

Table 2: Comparison of noise results

Point	Experimental results/dB	Simulation results/dB
A	122.18	120.42
B	126.39	125.14
C	122.67	121.41

3 Aerodynamic Noise Source

3.1 Noise Characteristics Analysis

Aerodynamic noise sources are derived from flow field data, rendering precise flow field data crucial for noise simulation. A simulation was conducted for a train model functioning at a low pressure of 0.05 atm, with a blockage ratio of 0.11, and an operation speed of 600 km/h. Fig. 8 depicts the distribution of the flow field along the longitudinal portion of the pipeline. The velocity distribution reveals a stagnation point at the front of the lead train, whereas the flow field surrounding the tail car is more intricate, displaying turbulence.

As the airflow traverses the streamlined intermediate car section, the cross-sectional area diminishes, resulting in a progressive increase in velocity. Ultimately, as the airflow moves through the streamlined posterior segment, the cross-sectional area expands, which leads to a reduction of flow velocity. The pressure distribution illustrated in Fig. 8b reveals that the peak positive pressure is located at the car's nose tip. Thereafter, the pressure progressively diminishes at the interface between the streamlined head car and the main body. The pressure variation is minimal along the middle car. As the cross-sectional area enlarges near the tail, the flow speed decreases, and the pressure increases.

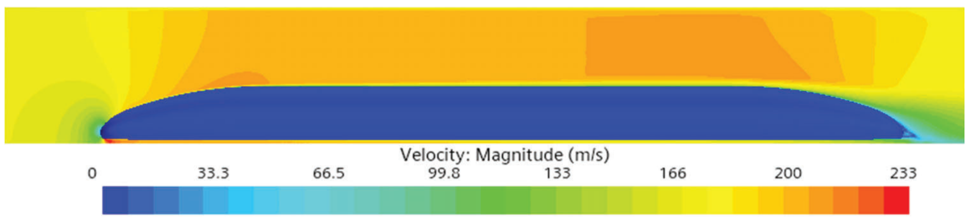

(a) velocity distribution

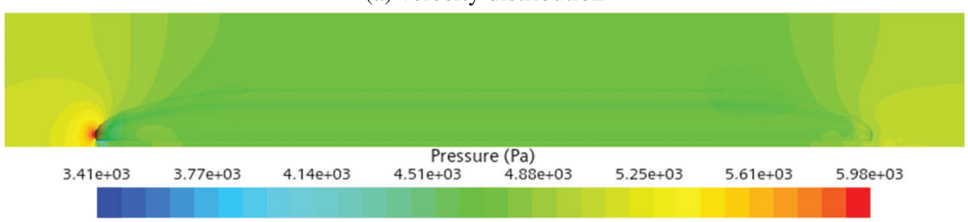

(b) pressure distribution

Figure 8: Flow field distribution

The results of the steady-state flow field study were utilized to implement the broadband noise source model for forecasting the distribution of noise sources on the train body surface. The computed data are represented in terms of surface sound power level and overall sound power level. The surface sound power level quantifies the intensity of dipole noise sources per a unit area of the train surface, generated by boundary layer turbulence. The sound power level measures the intensity of quadrupole noise sources per unit volume of the flow field, originating from isotropic turbulence around the train.

Fig. 9 illustrates the distribution of surface sound power levels on the train. The figure clearly indicates substantial fluctuations in surface sound power levels within the streamlined regions of the head and tail cars, reflecting heightened turbulence in these areas. The changes in surface sound power level are less pronounced in the middle car. The surface sound power level in the streamlined area of the head car is more than the tail car, with the maximal surface sound power level attaining 77 dB for the front car.

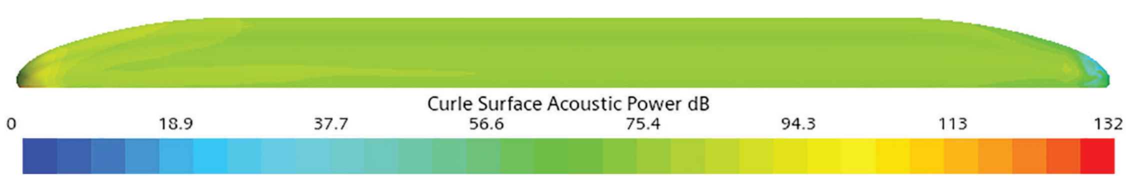

Figure 9: Distribution of surface sound power levels on the train

Fig. 10 illustrates the dispersion of the sound power level of the train. The sound power levels in the streamlined regions of the head and tail cars exhibit considerable variation, while the middle car shows less variation. The head car exhibits a maximum acoustic power level of 79 dB, somewhat exceeding the surface sound power level. The pipeline's presence induces compression and expansion of airflow at the front and rear of the train, leading to elevated sound power levels in the train's wake region.

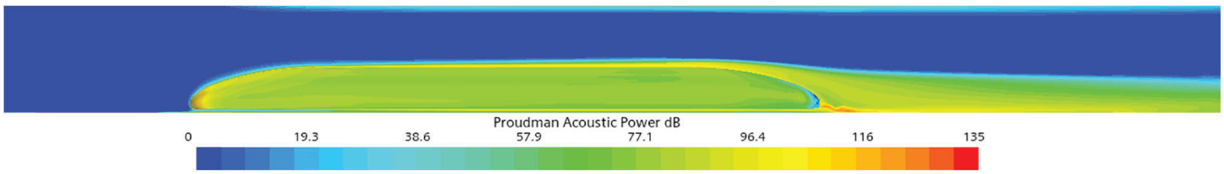

Figure 10: Distribution of sound power levels on the train

3.2 Analysis of the Impact of Speed

Fig. 11 depicts the distribution of sound sources along the longitudinal centerline (Line 1) of the train at different speeds, with an internal low-pressure level of 0.05 atm and a blockage ratio of 0.11. The distribution patterns of sound sources exhibit similarities at different speeds, with notable discrepancies in the streamlined areas of the head and tail cars, whilst the middle car demonstrates minimal variance. This phenomenon arises from the pipeline, which induces compression and expansion of airflow around the train's head and tail, leading to pronounced turbulence in these regions. As speed increases, both dipole and quadrupole noise sources of the train intensify. When the train travels at speeds of less than 1000 km/h, the sound source intensity in the streamlined area of the head car is greater than that of the tail car. As velocity escalates, the turbulence effects in the wake region intensifies, leading to higher sound source intensity at the tail. When the speed of the train is up to 1000 km/h, the sound intensity in the streamlined region of the tail car surpasses that in the head car. The dipole noise sources for the middle automobile are 77, 96, and 121 dB at varying speeds, but the quadrupole noise sources are 79, 108, and 132 dB, respectively. The intensity of quadrupole noise sources surpasses that of dipole noise sources, suggesting that At train operating speeds greater than 600 km/h, quadrupole noise sources progressively dominates in low-pressure tube maglev trains.

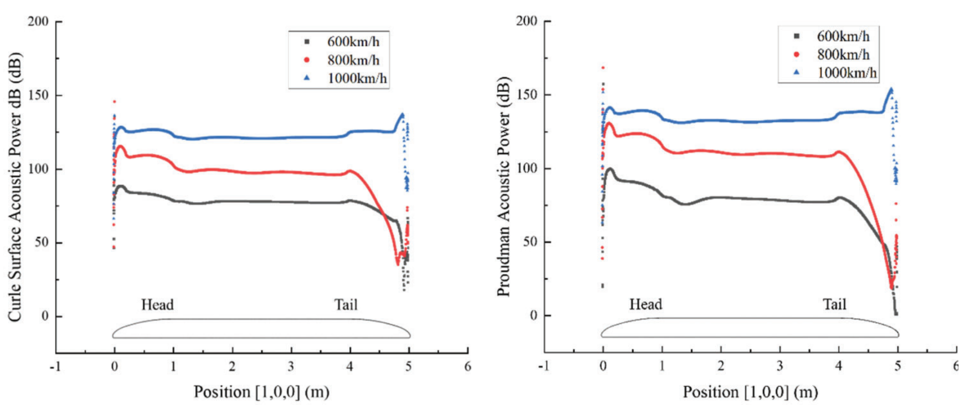

(a) dipole noise source (b) quadrupole noise source

Figure 11: Variation pattern of noise sources with train speed

3.3 Analysis of the Impact of Internal Low Pressure Level

Fig. 12 shows the distribution of sound sources along the longitudinal centerline (Line 1) of the train at different internal low-pressure levels, with a blockage ratio of 0.11 and a speed of 600 km/h. The distribution patterns of sound power levels remain consistent across different low-pressure levels, with notable fluctuations observed in the streamlined regions of the head and tail cars, whilst the middle car shows minimal variation. When the low-pressure level decreases from 0.2 to 0.01 atm, the air pressure diminishes, the gas density within the tube reduces, and the turbulence strength in the flow field lessens, resulting in a downward trend in the train's sound source. The average surface sound power levels of the middle car at different low-pressure levels are 103, 77, and 60 dB, respectively, while the sound power levels are 115, 79, and 40 dB, respectively. When the internal low pressure level ranges from 0.2 to 0.05 atm, the average sound power level of the middle car surpasses the surface sound power level, signifying that the intensity of quadrupole noise sources exceeds that of dipole noise sources. As the low-pressure level decreases, the disparity between quadrupole and dipole noise sources diminishes. When the low pressure level decreases to 0.01 atm, the sound power level of the train operating at 600 km/h becomes in general lower than the surface sound power level, and the intensity of quadrupole noise sources significantly weakens. The pipeline's presence amplifies the fluid's turbulent motion around the train body, while decreasing the internal low pressure significantly mitigates aerodynamic noise in low-pressure tube trains.

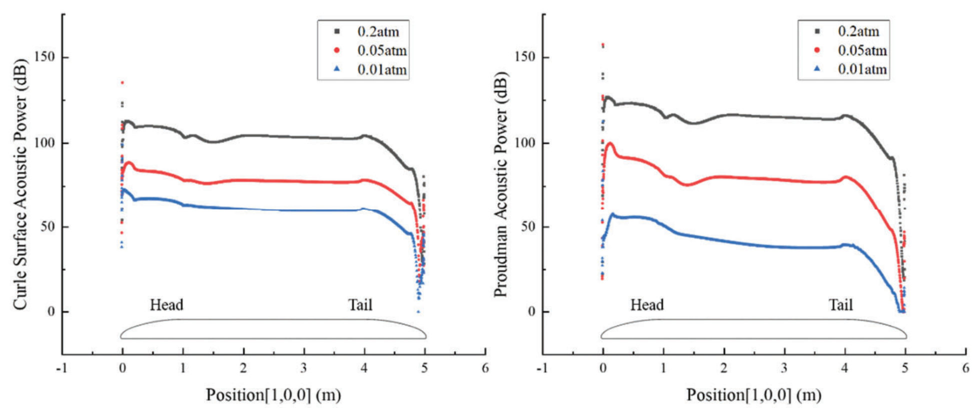

(a) dipole noise source (b) quadrupole noise source

Figure 12: Variation patterns of noise sources with internal low pressure level

4 Quantitative Impact Study

4.1 Quantitative Study of Velocity

This study concentrates on the average noise source values of the middle car for quantitative impact analysis, as the substantial changes in noise from the head and tail cars render them inadequate as reference points. According to Reference [26], there is a discernible relationship between the sound power level of the train L and the logarithm of its speed, and the relationship can be expressed as:

$$L = a + b\log(v/v_0) + c[\log(v/v_0)]^2 \tag{10}$$

In the equation, v represents the operational speed of the train, v_0 denotes the reference speed, which is specified as 600 km/h in this study, and a, b, and c are the regression coefficients.

Table 3 provides the average surface sound power level and sound power level of the middle car at various train speeds, with a low-pressure level of 0.05 atm and a blockage ratio of 0.11. By substituting these results into Eq. (10) and applying the least squares approach to ascertain the unknown parameters, the values of a, b, and c may be individually determined. This enables the derivation of the relationship between the dipole noise source L_{SA} and quadrupole noise sources L_A and the operating speed of the train.

$$L_{SA} = 77 + 92.50\log(v/v_0) + 477.35[\log(v/v_0)]^2 \tag{11}$$

$$L_A = 79 + 223.46 + \log(v/v_0) + 69.85[\log(v/v_0)]^2 \tag{12}$$

The fitted formula indicates that at a train speed of v = 700 km/h, the dipole sound source level L_{SA} is 85 dB and the quadrupole sound source level L_A is 94 dB. Numerical simulations, in contrast, yield a dipole sound source level of 82 dB and a quadrupole sound source level of 91 dB for the middle car, with an error margin of less than 3.6%. The comparison with the results presented in Fig. 13 demonstrates that the fitting is highly precise. Therefore, the formula can be effectively used to predict noise levels within the range of 600 to 1000 km/h, providing a valuable reference for pertinent study.

Table 3: Sound source values of the middle car at different running speeds

Speed (km/h) Sound source (dB)	600	800	1000
Dipole noise source	77	96	121
Quadrupole noise source	79	108	132

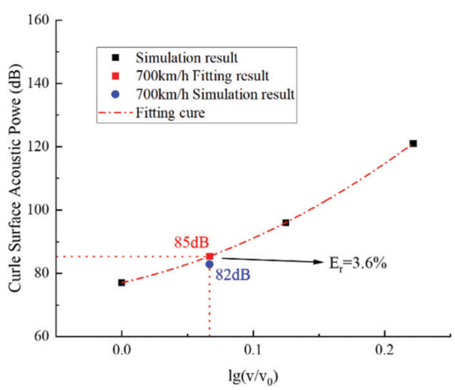

(a) dipole noise source

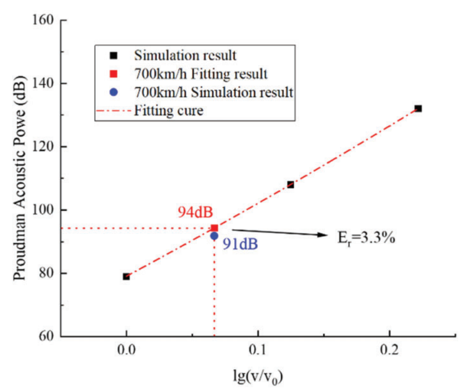

(b) quadrupole noise source

Figure 13: Relationship between noise sources and train running speed

4.2 Quantitative Study of Low-Pressure Level

Alterations in the low-pressure level within the pipeline will result in modifications to the gas density and sound speed. The relationships between the pressure, sound speed, and density of an ideal gas are described by the following equations:

$$p = \rho_0 RT \tag{13}$$

$$c_0^2 = \frac{B}{\rho_0} \tag{14}$$

In these equations, R denotes the molar gas constant, T represents the gas temperature, and B signifies the bulk modulus of the gas.

Combining Eqs. (3) and (6), the relationship between the sound power level of the train L and the logarithm of the internal pipeline pressure can be shown as follows:

$$L = d + e\log(p/p_0) + f[\log(p/p_0)]^2 \tag{15}$$

In the equation, p represents the internal pipeline pressure, p_0 denotes the reference pressure (set to 0.01 atm in this study), and d, e, and f are the regression coefficients.

The average surface sound power level and sound power level of the middle car at different low-pressure levels within the pipeline, with a train speed of 600 km/h and a blockage ratio of 0.11, are displayed in Table 4. By entering these values into Eq. (15) and applying the least squares approach, the unknown parameters d, e, and f can be determined. This allows for the derivation of the relationship between the dipole noise sources L_{SA} and quadrupole noise sources L_A and the low-pressure level inside the tube.

$$L_{SA} = 60 + 15.17\log(p/p_0) + 13.75[\log(p/p_0)]^2 \tag{16}$$

$$L_A = 40 + 55.30\log(p/p_0) + 1.80[\log(p/p_0)]^2 \tag{17}$$

According to the fitted formula, at an internal pipeline low pressure level of $p = 0.1$ atm, the dipole sound source level L_{SA} is 89 dB, whereas the quadrupole sound source level L_A is 97 dB. Numerical simulations show that the dipole and quadrupole sound source levels for the intermediate cars are 89 and 99 dB, respectively, with a margin of error of 2%, and the comparison results are shown in Fig. 14. The fitting is precise and serves as a significant reference, facilitating accurate predictions of aerodynamic noise for low-low pressure tube maglev trains.

Table 4: Sound source values of the middle car at different low pressure levels

Pressure (atm) Sound source (dB)	0.01	0.05	0.2
Dipole noise source	60	77	103
Quadrupole noise source	40	79	115

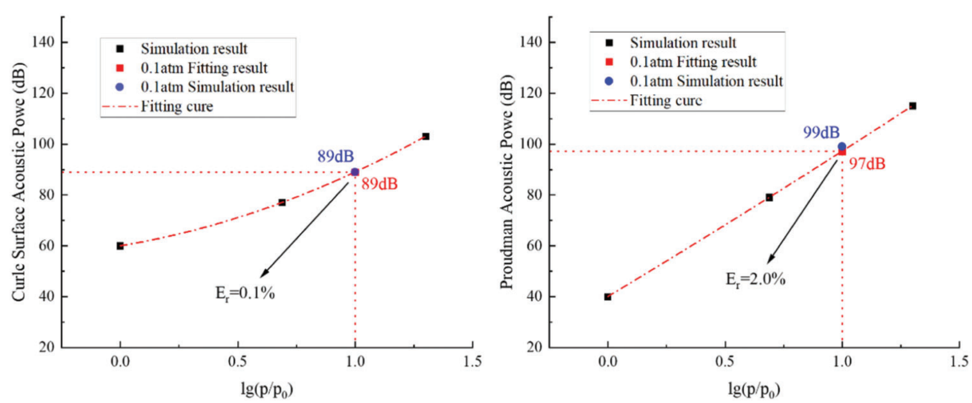

(a) dipole noise source (b) quadrupole noise source

Figure 14: Relationship between noise sources and low pressure levels

5 Conclusions

This paper develops a numerical calculation model for analyzing the outflow field of an ultra-high-speed maglev train operating in a low-low pressure tube. Employing a broadband noise source model, we analyze the aerodynamic noise characteristics of the train and investigate the influence of train speed and tube low pressure level on noise sources. The following conclusions were reached:

(1) The disparity in sound sources between the streamlined sections of the head and tail cars of the low-pressure tube maglev train is considerable, but it is lesser for the middle car. The presence of the pipeline compresses and expands the airflow at the train's head and tail, leading to a higher sound source intensity in the train wake region.

(2) Train sound source increases with speed in low low-pressure pipes. Progressive predominance of quadrupole sound sources in low-low pressure tube magnetic levitation trains at speeds greater than 600 km/h. Trains running at speeds below 1000 km/h, the sound source intensity in the streamlined regions of the head car exceeds that of the tail car. The intensity of the streamlined area sound source in the rear of the train exceeds that of the lead car when the train's speed reaches 1000 km/h.

(3) In the low-low pressure tube, the sound source of the train decreases as the low-pressure level decreases. When the low-pressure level is reduced to 0.01 atm, the quadrupole sound source strength of a train traveling at 600 km/h significantly weakens and falls below that of the dipole sound source. Reducing the low-pressure level within the tube has a notable impact on mitigating the aerodynamic noise of the low-low pressure tube train.

(4) This study quantitatively assesses the characteristics of noise sources in ultra-high-speed maglev trains operating in low-pressure tubes. Mathematical equations were formulated to characterize the correlation among train speed, tube low-pressure levels, and noise sources, yielding a fit for the numerical simulation outcomes. The maximum error of the fit is within 3.6%, enabling effective prediction of aerodynamic noise for low-pressure tube maglev trains.

Acknowledgement: The authors sincerely acknowledge the contributions of all participants for their dedicated efforts, as well as the invaluable support provided by the anonymous reviewers and journal editors.

Funding Statement: This study was funded by the Talent Program (Ph.D. Fund) of Chengdu Technological University (grant number 2024RC025), the Natural Science Foundation of Sichuan Province (grant number 2022NSFSC1892) and Fundamental Research Funds for the Central Universities (grant number XJ2021KJZK054).

Author Contributions: The authors confirm contribution to the paper as follows: study conception and design: Lanxi Zhang, Yudong Wu, Yuming Peng; data collection: Lanxi Zhang, Yudong Wu; analysis and interpretation of results: Lanxi Zhang; draft manuscript preparation: Lanxi Zhang; manuscript review: Yudong Wu, Yuming Peng. All authors reviewed the results and approved the final version of the manuscript.

Availability of Data and Materials: The data used to support the findings of this study are available from the corresponding author upon request.

Ethics Approval: Not applicable.

Conflicts of Interest: The authors declare no conflicts of interest to report regarding the present study.

References

1. Zhang J, Wu YW, Gao JY, Gao GJ, Yang ZG. Study on aerodynamic noise characteristics of a high-speed maglev train with a speed of 600 km/h. Railw Sci. 2023;2(3):310–26.

2. Yao Y, Sun Z, Li G, Yang G, Prapamonthon P, Guo Y, et al. Aerodynamic optimization using passive control devices near the bogie cabin of high-speed trains. Acta Mechanica Sinica. 2022;38(9):321363 (In Chinese). doi:10.1007/s10409-022-21363-x.
3. Sang H, Zeng J, Wang Q, Huang C, Mu J, Qi Y, et al. Theoretical study on wheel wear mechanism of high-speed train under different braking modes. Wear. 2024;540–1.
4. Wang XF, Hu X, Li ZP, Liu JR, Deng ZG, Zhang WH. The effect of track structure on the aerodynamic characteristics of evacuated tube maglev train. J Exp Fluid Mech. 2023;37(3):9–18 (In Chinese).
5. Tan X, Wang T, Qian B, Qin B, Lu Y. Aerodynamic noise simulation and quadrupole noise problem of 600 km/h high-speed train. IEEE Access. 2019;7:124866–75. doi:10.1109/Access.6287639.
6. Liu X, Zhang J, Thompson D, Iglesias EL, Squicciarini G, Hu Z, et al. Aerodynamic noise of high-speed train pantographs: comparisons between field measurements and an updated component-based prediction model. Appl Acoust. 2021;175:107791. doi:10.1016/j.apacoust.2020.107791.
7. Liu ZJ, Li XR, Cui XP. Numerical analysis of the surface aerodynamic noise of the CRH3 high speed train. Adv Mater Res. 2014;3530(1044–1045):643–9.
8. Tan X, Gong L, Zhang X, Yang Z. Influence of ground effect on flow field structure and aerodynamic noise of high-speed trains. J Zhejiang Univ-Sci A. 2024;25(2):147–60 (In Chinese). doi:10.1631/jzus.A2300034.
9. Shi J, He Y, Zhang J, Li T. Effect of geometry simplification and boundary condition specification on flow field and aerodynamic noise in the train head and bogie region of high-speed trains. J Zhejiang Univ-Sci A. 2024;25:716–31. (In Chinese). doi:10.1631/jzus.A2300307.
10. Li T, Qin D, Zhou N, Zhang JY, Zhang WH. Numerical study on the aerodynamic and acoustic scale effects for high-speed train body and pantograph. Appl Acoust. 2022;196:108886. doi:10.1016/j.apacoust.2022.108886.
11. Liu JL, Zhang JY, Zhang WH. Simulation of noise source for high speed train in evacuated tube. Chin J Vac Sci Technol. 2013;33(10):1026–31 (In Chinese).
12. Zhang KR, Li QL, Wang CW, Jia WG. Aerodynamic noises of low pressure tube transportation: a simulation and theoretical study. Chin J Vac Sci Technol. 2019;39(11):950–6 (In Chinese).
13. Liu JL, Yu MG, Chen DW, Yang ZG. Study on interior aerodynamic noise characteristics of the high-speed maglev train in the low low pressure tube. Appl Sci. 2022;12(22):11444. doi:10.3390/app122211444.
14. Shen C. Rarefied gas dynamics: fundamentals, simulations and micro flows. China: Springer Science & Business Media; 2006.
15. Huang Z, Liang X, Chang N. Analysis on simulation algorithm for train outflow field of low pressure pipeline traffic. J Eng Thermophys. 2018;39(6):1244–50 (In Chinese).
16. Zhong S, Qian S, Yang Z, Wu F, Wang TT, Tan CD, et al. Investigation on flow field structure and aerodynamic load in low pressure tube transportation system. J Wind En Indust Aerodyn. 2021;215:104681. doi:10.1016/j.jweia.2021.104681.
17. Shih TH, Liou WW, Shabbir A, Yang Z, Zhu J. A new k-ε eddy viscosity model for high reynolds number tubulent flows. Comput Fluids. 1995;24(3):227–38. doi:10.1016/0045-7930(94)00032-T.
18. Ma C, Wang HM, Jia WG. Influence of cross-pass piping parameters on the running resistance of low pressure tube trains. Chin J Low Press Sci Technol. 2023;43(2):124–33 (In Chinese). doi:10.13922/j.cnki.cjvst.202204025.
19. Lighthill MJ. On sound generated aerodynamically. I. General theory. Proc Royal Soc London. Series A, Math Phy Sci. 1952;211(1107):564–87.
20. Ffowcs-Williams JE, Hawkings DL. Sound generation by turbulence and surfaces in arbitrary motion. Philos Trans Royal Soc London. Series A, Math Phys Sci. 1969;264(1151):321–42.
21. Shi JW, Zhang JY. Effect of bogie cavity end wall inclination on flow field and aerodynamic noise in the bogie region of high-speed trains. Comput Model Eng Sci. 2024;139(2):2175–95. doi:10.32604/cmes.2023.043539.
22. Curle N. The influence of solid boundaries upon aerodynamic sound. Proc Royal Soc London. 1955;231(1187):506–14.
23. Proudman I. The generation of noise by isotropic turbulence. Proc Royal Soc London. Series A, Math Phys Sci. 1952;214:119–32. doi:10.1098/rspa.1952.0154.

24. Tan C, Zhou D, Chen G, Sheridan J, Krajnovic S. Influences of marshalling length on the flow structure of a maglev train. Int J Heat Fluid Flow. 2020;85(12):108604. doi:10.1016/j.ijheatfluidflow.2020.108604.
25. Meng S, Zhou D, Meng S. Effect of rail gap on aerodynamic performance of maglev train. J Cent South Univ (Sci Technol). 2020;51:3537–45 (In Chinese).
26. Mellet C, Létourneaux F, Poisson F, Talotte C. High speed train noise emission: latest investigation of the aerodynamic/rolling noise contribution. J Sound Vib. 2005;293(3):535–46.